al Kimiya: Jurnal Ilmu Kimia dan Terapan,
p-ISSN: 2407-1897, e-ISSN: 2407-1927
Vol. 11, No. 1 (51-60), June 2024/Djulhijah 1445

URINE GLUCOSE DETECTION VIA GOLD NANOPARTICLE FORMATION USING 3D-CONNECTOR MICROFLUIDIC PAPER-BASED ANALYTICAL DEVICES

KRISTA FIRDAUS SUWARNO PUTRI[1], HERMIN SULISTYARTI[1], AND AKHMAD SABARUDIN[1*]

[1]Department of Chemistry, Faculty of Mathematics and Natural Sciences, Universitas Brawijaya, Veteran street, Malang 65145, Indonesia

*Corresponding Author email: sabarjpn@ub.ac.id

Article Information

Received: Feb 29, 2024
Revised: May 25, 2024
Accepted: Jun 10, 2024
Published: Jun 29, 2024

DOI: 10.15575/ak.v11i1.35245

Keywords:
Diabetes mellitus; glucose; μPADs; AuNPs; non-invasive

Abstract

A metabolic disorder that has experienced a significant increase in the world is diabetes mellitus. Diabetes is caused by two main factors: the first is damage to pancreatic beta cells, which prevents insulin from being produced, and the second is impaired insulin secretion and function. Chronic diabetes, if not treated properly, can lead to acute complications including eye, kidney, lung, nerve, and even death. Diabetes can be diagnosed through blood and urine. In general, glucose detection is carried out using invasive methods that use blood samples, which can cause pain and discomfort for users. Current research is developing non-invasive glucose detection using urine samples. This research aims to develop non-invasive glucose detection technology using 3D-connector μPADs (Microfluidic Paper Based Analytical Devices) which have the advantages of being safe, easy, and simple. The three-dimensional connector on the device functions as a connector to facilitate the coordination of fluid flows in the sample zone and detection zone. The glucose detection method uses gold (III) chloride as a gold nanoparticle (AuNPs) precursor, an aqueous extract of Acalypha indica Linn as a stabilizing agent, sodium hydroxide (NaOH) as a catalyst, and glucose in artificial urine as a sample. Method validation results using imageJ software indicated linearity with a coefficient of determination value (R^2) of 0.9714, precision with a %RSD value (Relative Standard Deviation) of 2.69, and an accuracy level ranging from 92.22-99.23%.

INTRODUCTION

Diabetes mellitus is a complex metabolic condition characterized by high blood sugar levels (hyperglycemia) caused by insulin production or its effectiveness [1]. Insulin is crucial in regulating blood glucose levels, glucose assimilation, and utilization. Insulin resistance, experienced by individuals with diabetes mellitus lead body cells to reject insulin hormone, accumulating glucose in the bloodstream [2]. Diabetes is divided into three primary types: type 1 diabetes, type 2 diabetes, and gestational diabetes induced by pregnancy [3]. According to the International Diabetes Federation (IDF), In 2017, there were 451 million adults living with diabetes worldwide. Diabetes is estimated to impact 693 million individuals by 2045 if not properly managed and prevented, despite many efforts to increase life expectancy [4].

Excessive consumption of sugary foods and an unhealthy lifestyle are contributing factors to diabetes, leading to an increased Body Mass Index (BMI). Individuals with a higher BMI are more likely to develop type 2 diabetes [5]. Besides BMI, the characteristics of diabetes patients include having blood glucose levels that reach ≥ 126 mg/dL [6]. According to the American Diabetes Association, individuals with diabetes mellitus need to preserve blood glucose by strictly controlling blood glucose levels below 10 mmol/L (180 mg/dL). Failure to comply can lead to serious complications including vision impairment, kidney damage, stroke, cardiovascular issues, liver problems, coma, and death. Regular blood glucose level monitoring is essential for medical diagnosis and preventing complications due to hyperglycemia, especially in diabetic individuals [7-8]. Early detection of glucose levels in individuals with diabetes mellitus could be performed using both invasive and non-invasive methods. The invasive method requires blood samples, which can cause pain due to tissue damage, while the non-invasive method employs samples other than blood, such as interstitial fluid, urine, sweat, saliva, and tears, thus eliminating pain [9].

Microfluidic Paper-Based Analytical Devices (μPADs) hold an immense potential for the development of Point-of-Care Testing (POCT), the first concept was proposed by

Whitesides in 2007 [10-11]. µPADs as glucose detection devices fulfill the WHO (World Health Organization) "ASSURED" criteria, namely Affordable, Sensitive, Specific, User-friendly, Robust and rapid, Equipment-free, and Deliverable to individuals with diabetes melitus [12]. The fabrication of µPADs has undergone significant advancements, including their potential as visually based detection devices (colorimetry) [13-14], electrochemistry [14], chemiluminescence [15], fluorescence [16], and Raman spectroscopy [17]. µPADs as glucose detection devices could be categorized into two types: the colorimetric method and the distance-based method. The colorimetric method utilizes µPADs designs by observing the formed color without determining the distance of reaction, while the distance-based method involves measuring the distance based on the length of the generated color band. Influencing factors of µPADs analysis include color intensity calculation and lighting effects, which affect sensitivity and reproducibility [18].

The detection system used in µPADs is based on the formation of nanoparticles such as gold and silver. These nanoparticles play a role in inducing color changes that occur on the µPADs [19]. Gold nanoparticles (AuNPs) are widely employed as catalysts due to their excellent biocompatibility, high stability, and low cytotoxicity [21], drug delivery [22], biosensors [23], cancer photothermal therapy [24], bioelectric devices [25], dan x-ray imaging [26]. The presence of glucose in diabetic mellitus patients can be detected using gold nanoparticles [27]. Gold nanoparticles are employed as sensing components due to their unique physicochemical and optical properties, ranging from their shape and surface characteristics to their size, which falls within the range of 1-100 nm [20]. In light of the rising prevalence of diabetes mellitus, particularly in underdeveloped and developing countries, the development of 3D-Connector µPADs based on the distance-based reaction method holds promise as a reliable breakthrough for rapid, cost-effective, and safe glucose detection.

EXPERIMENT

Material

The materials used for this research include Whatman Number 1 chromatography paper from Cytiva (China), D-(+)-Glucose (Merck), sodium hydroxide (Germany. Sigma Aldrich), gold (III) chloride (Smart Lab, 49%), and Acalypha indica Linn. The reagents used in the artificial urine solution, namely citric acid monohydrate (98%) sodium bicarbonate (99,5-100%), uric acid (99%), sodium chloride (99%), sodium sulfate decahydrate (99%), potassium phosphate monobasic (99%), potassium phosphate dibasic trihydrate (99%), ammonium chloride (99,5%), lactic acid (99%), calcium chloride (99%), magnesium sulfate (99%), and urea (98%), were obtained from Sigma Aldrich. Distilled water is used as a solvent in the experiment.

Instrumentation

The instrumentation used in this research included a Xerox ColorQube 8580 DN printer, solid ink color for fabricating 3D-µPADs, an oven for wax penetration into the paper substrate, and CorelDRAW Graphics Suite X7 software for designing the 3D-µPADs. Image capture was performed using a black box equipped with LED lights measuring 10x10x10 cm, LED lights, and a 12MP mobile phone camera with 2x magnification.

Procedure

Fabrication of 3D-µPADs

Fabrication of 3D-Microfluidic Paper-Based Analytical Devices (µPADs) involved designing the µPADs using CorelDRAW Graphics Suite X7 and printing them onto Whatman Number 1 paper using Xerox ColorQube 8580 DN printer. After printing, wax penetration was performed on the paper substrate by heating it in an oven at 120°C for 3 minutes to maximize the formation of a hydrophobic barrier on the 3D-µPADs. Subsequently, the paper was cut according to the design using a paper trimmer and scissor. The fabrication process of the 3D-µPADs is illustrated in **Figure 1.**

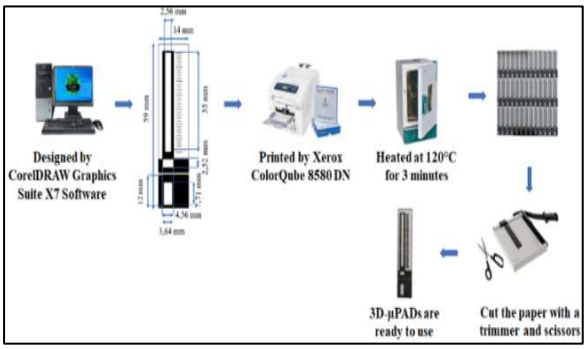

Figure 1. 3D-µPADs fabrication schematic illustration.

In-situ Synthesis of AuNPs on 3D-μPADs

In-situ synthesis of AuNPs on 3D-μPADs is depicted in **Figure 2.** 10 μL solution of 100 mM gold (III) chloride ($HAuCl_4$) and *Acalypha indica* Linn aqueous extract 0.25% (5:1 volume ratio) was evenly dropped onto the detection zone from bottom to top then dried for 15 minutes at room temperature. A 0.25% extract of Acalypha indica Linn was prepared by mixing 5 g of Acalypha indica Linn powder with 200 g of distilled water, then stirred and heated at 60°C for 20 minutes.

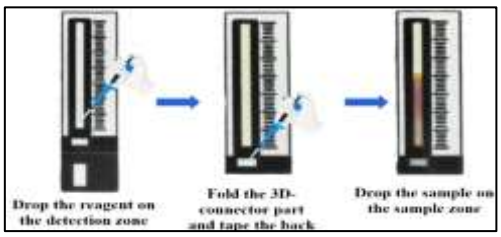

Figure 2. In-situ synthesis of AuNPs on 3D-μPADs.

Subsequently, the 3D-connector was folded and sealed with transparent tape and clamped with acrylic to maximize the reaction distance efficiency. After folding, a 20 μL sample containing 100 mg/dL glucose in artificial urine and 10 M NaOH was dropped onto the detection zone and dried for 15 minutes at room temperature. The color change and length of the reaction distance were observed for 15 minutes. Data were collected through analysis using ImageJ software by calculating the slope value (y/x) based on **Equation 1** and **Figure 3.**

$$\text{Slope } (y/x) = \frac{(y2 - y1)}{(x2 - x1)} \quad (1)$$

A clear color boundary is indicated by a high slope value. The blue color intensity is chosen because the slope value of the blue color intensity is higher than those of the red and green colors in the ImageJ analysis.

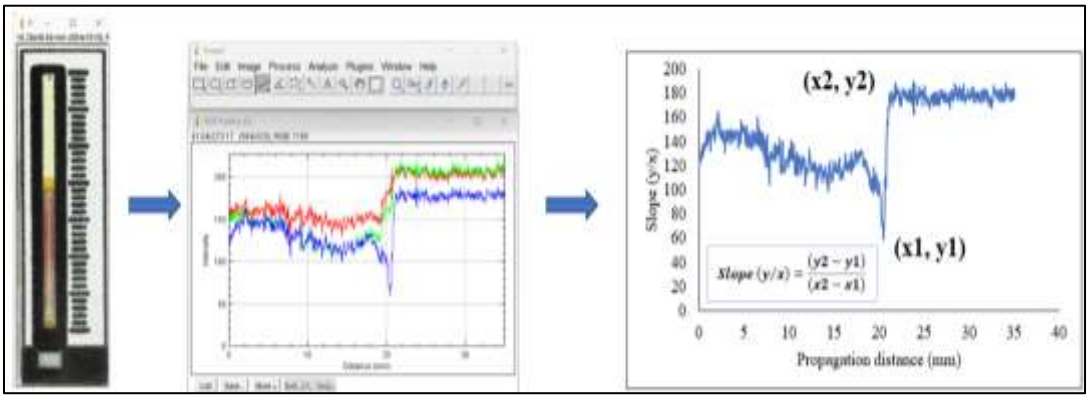

Figure 3. Data acquisition using ImageJ.

Validation Method

Validation method was performed after obtaining the optimal conditions from the optimization of reagent volume, sample volume, drying time, reagent concentration, and reaction time. Method validation included linearity, precision, and accuracy. Linearity measurement is performed using artificial urine with the composition shown in **Table 1** with standard glucose analyte concentrations of 0, 20, 40, 60, 80, and 100 mg/dL. Then the obtained data are processed to obtain SD (Standard Deviation) and %RSD (Relative Standard Deviation). Precision determination is carried out by measuring the concentration of standard glucose analyte 100 mg/dL for six times. Accuracy is determined by measuring the concentration of standard glucose analyte in artificial urine 15, 25, 50, and 75 mg/dL, then compared to the previous standard glucose analyte at equivalent concentrations.

Table 1. Composition of artificial urine solutions.

Composition of solution	Concentration (mM)
Citric acid	2
Sodium bicarbonate	25
Uric acid	0.4
Sodium chloride	90
Sodium sulfate decahydrate	10
Potassium phosphate monobasic	7
Potassium phosphate dibasic trihydrate	7
Ammonium chloride	25
Lactic acid	1.1
Calcium chloride	2.5
Magenisum sulfate	2
Urea	170

RESULT AND DISCUSSION

Effect of Wax Penetration On 3D-Mpads

Wax penetration into the 3D-μPADs serves to create a hydrophobic barrier on the paper substrate, thereby optimizing the solution permeation process. During the wax heating process, there is a narrowing of the detection zone, sample zone, and 3D connector as shown in **Table 2**. Based on the results of wax penetration measurements, there is the narrowing of the detection zone to (0.89 x 0.69) mm, the sample zone to (0.77 x 0.76) mm, and the 3D connector zone to (0.86 x 0.8) mm.

Table 2. Measurement of wax penetration on 3D-μPADs.

Repetition	Detection Zone		Sample Zone		3D-Connector	
	Length	Width	Length	Width	Length	Width
1	34.17	1.86	3.78	1.77	6.76	2.77
2	34.17	1.87	3.81	1.71	6.76	2.83
3	34.26	1.89	3.75	1.75	6.89	2.80
4	34.04	1.89	3.85	1.74	6.83	2.86
5	33.97	1.88	3.76	1.77	6.91	2.90
6	34.03	1.85	3.77	1.79	6.93	2.88
Average	34.11	1.87	3.79	1.76	6.85	2.84
SD	0.11	0.02	0.04	0.03	0.08	0.05
%RSD	0.32	0.87	0.98	1.60	1.10	1.74

In Situ Synthesis of Gold Nanoparticles (AuNPs)

In-situ synthesis of AuNPs is carried out using $HAuCl_4$ precursor, Acalypha indica Linn aqueous extract as a stabilizer, NaOH as a catalyst, and glucose as a reductant, which takes place in-situ on 3D-μPADs. 3D-connectors in μPADs control fluid flow by connecting and separating reagent and sample fluids, thereby enhancing the detection accuracy and performance of 3D μPADs. The purpose of folding the 3D connector part is to prevent air contamination and accelerate the reaction distance of the sample solution. The order of dropping is determined based on the detectable color change and length of the reaction distance. Glucose, which plays a role in reducing Au^{3+} to Au^0, binds to the surface of gold nanoparticles through hydrogen bonding of hydroxyl groups (OH^-). AuNPs cannot form under acidic conditions, hence NaOH is required to create a basic environment [28]. Detection of glucose through the formulation of AuNPs is as follows [29].

$$C_5H_{11}O_5CHO + 3OH^- \rightarrow C_5H_{11}O_5COO^- + 2H_2O + 2e^-$$

$$HAuCl_4 + 3e^- \rightarrow Au^0 + H^+ + 4Cl_4$$

$$3C_5H_{11}O_5CHO + 9OH^- + 2HAuCl_4 \rightarrow 2Au^0 + 3C_5H_{11}O_5COO^- + 6H_2O + 2H^+ + 8Cl^-$$

Determination of Reagent Volume

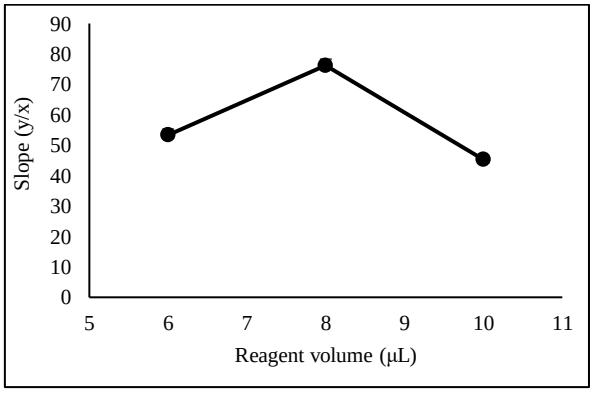

(a)

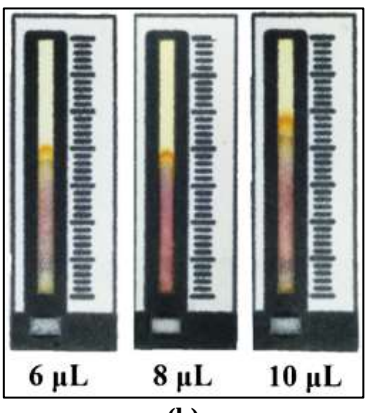

(b)

Figure 4. (a) Graph of the relationship between the average slope value (y/x) and the reagent volume, (b) 3D-μPADs image for reagent volume optimization.

The reagent used is a mixture of $HAuCl_4$ solution and Acalypha indica Linn aqueous

extract. The results of the reagent volume optimization can be seen in **Figure 4**. Visually, there is an increase in color sharpness from 6 µL to 8 µL reagent volume, followed by a decrease at 10 µL volume. The optimum reagent volume is 8 µL. The observation results are consistent with the ImageJ analysis, which shows the color sharpness threshold. The slope value measurement is performed three times using ImageJ software. The color formed at 8 µL volume is sharper than at 10 µL volume. At 10 µL volume, the color appears uneven, which is caused by the increasing amount of fluid accommodated in the detection zone, leading to a decrease in the formation of gold nanoparticles (AuNPs) and affecting the color sharpness.

Determination of Sample Volume

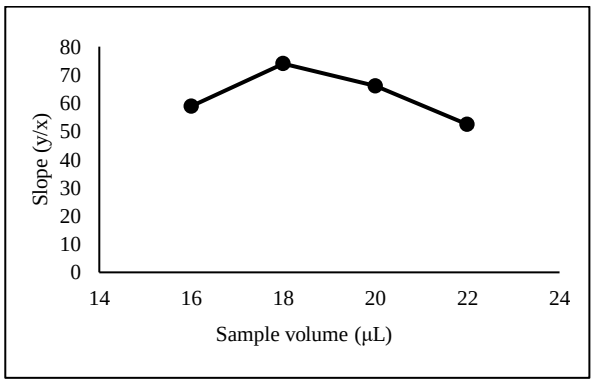

(a)

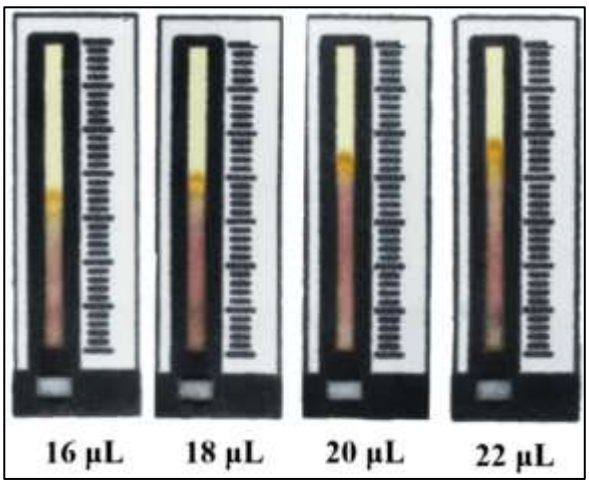

(b)

Figure 5. (a) Graph of the relationship between the average slope value (y/x) and the sample volume, (b) 3D-µPADs image for sample volume optimization.

Sample volume determination is performed to identify the optimal sample volume from the mixture of glucose solution in artificial urine and NaOH. The results of the sample volume optimization can be seen in **Figure 5**. The observations reveal that the length of the reaction distance increases as the sample volume rises. The optimum sample volume is 18 µL. The color sharpness threshold starts to decrease when the sample volume is 20 µL and 22 µL. The decrease in color sharpness is attributed to the increased fluid volume in the sample zone, which prolongs the reaction time for gold nanoparticle (AuNPs) formation, leading to an indistinct color change threshold.

Determination of Reagent Drying Time

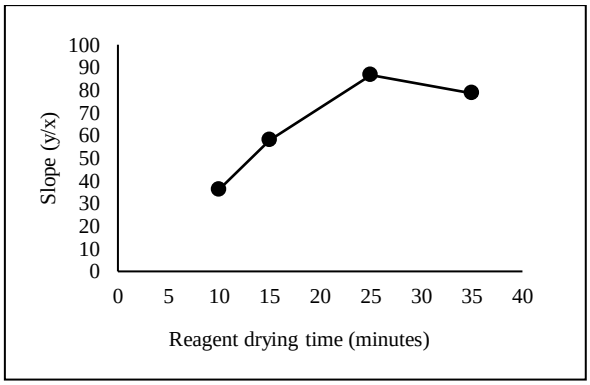

(a)

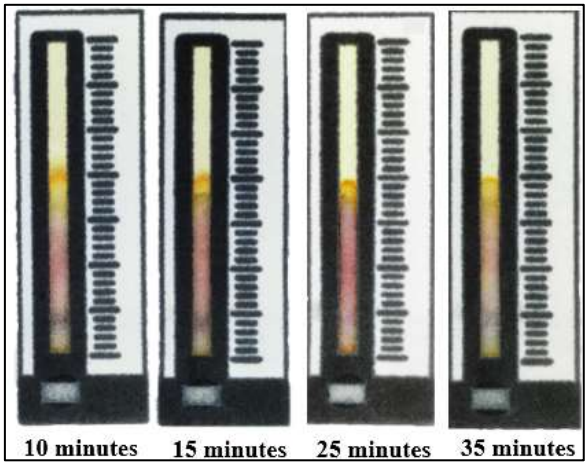

(b)

Figure 6. (a) Graph of the relationship between the average slope value (y/x) and the reagent drying time, (b) 3D-µPADs image for reagent drying time optimization.

The determination of reagent drying time is employed to identify the optimal drying time for the mixture of $HAuCl_4$ solution and Acalypha indica Linn aqueous extract applied to the detection zone with equal reagent and sample volumes. The results of the reagent drying time optimization are shown in **Figure 6**. The optimum reagent drying time is 25 minutes. The color

sharpness produced at a reagent drying time of 10 minutes is fainter compared to 15 minutes. Color sharpness increases with increasing drying time from 10, 15, to 25 minutes. The drier the detection zone, the more AuNPs will form, as indicated by a sharper color threshold. At 15 and 25 minutes of drying time, the resulting color appears similar, but the color sharpness threshold at 25 minutes appears more even and sharper. This color sharpness enhancement ceases at 35 minutes when the resulting color is fainter.

Determination of Gold (III) Chloride Concentration

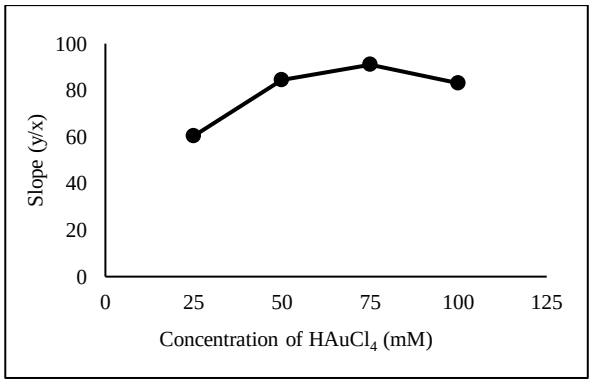

(a)

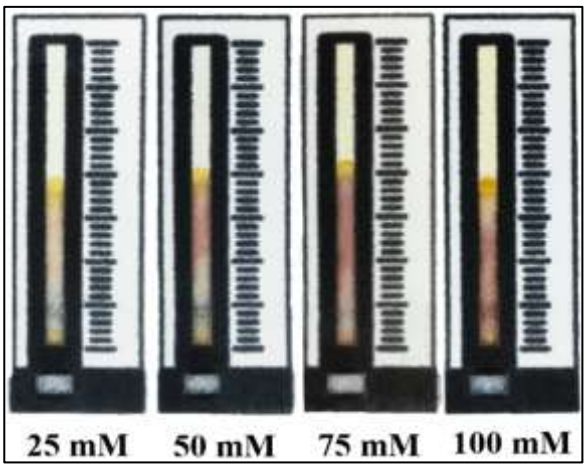

(b)

Figure 7. (a) Graph of the relationship between the average slope value (y/x) and the concentration of gold (III) chloride, (b) 3D-μPADs image for gold (III) chloride concentration.

The determination of gold (III) chloride ($HAuCl_4$) precursor concentration aims to identify the amount of AuNPs formed. The results of the concentration of $HAuCl_4$ optimization are shown in **Figure 7**. The optimum $HAuCl_4$ precursor concentration is 75 mM. The color observed at 25 mM $HAuCl_4$ concentration is fainter compared to concentration of 50 mM. This indicates that at low concentrations, gold nanoparticles are not fully formed, resulting in an invisible color. As the $HAuCl_4$ concentration increases, the color sharpness threshold or slope also increases. At $HAuCl_4$ concentration of 25 mM, there is a significant increase to 50 mM, demonstrating that $HAuCl_4$ plays a significant role in AuNPs formation and consequently influences color sharpness. The color sharpness threshold increases up to 75 mM concentration and then decreases at 100 mM.

Determination of NaOH Concentration

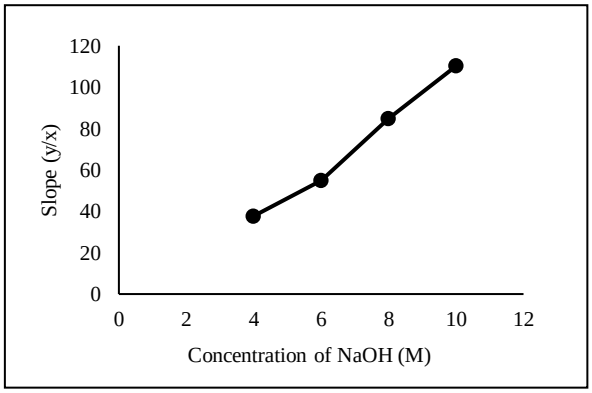

(a)

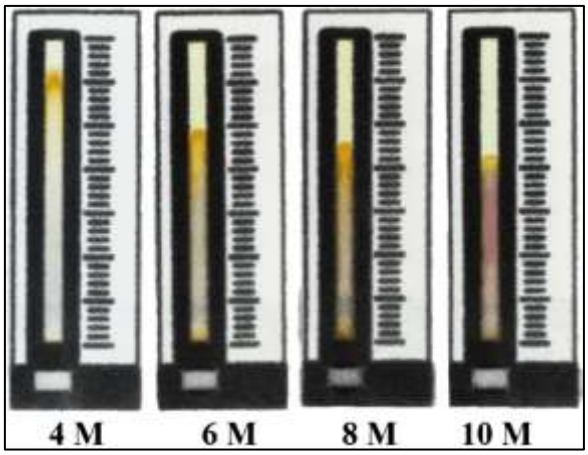

(b)

Figure 8. (a) Graph of the relationship between the average slope value (y/x) and the concentration of NaOH, (b) 3D-μPADs image for NaOH concentration.

The determination of NaOH concentration aims to investigate the influence of NaOH on AuNPs formation. NaOH, acting as a catalyst, plays a crucial role in enhancing color sharpness and length of the reaction distance. The results of the NaOH concentration optimization are shown in **Figure 8**. The colors produced at NaOH concentrations of 4, 6, and 8 M are extremely faint and almost invisible, making observation challenging. This indicates that as NaOH

concentration decreases, AuNP formation diminishes due to the hindered glucose reduction reaction in converting Au^{3+} to Au^{0}. AuNP formation is more effective in alkaline conditions [29]. The optimum NaOH concentration is 10 M. The optimal concentration of NaOH is 10 M due to the solubility of NaOH in water being 1 g/L at 25°C. At 4 M NaOH concentration, the length of the reaction distance is high but decreases at 6, 8, and 10 M NaOH concentrations. As the NaOH concentration increases, the resulting color becomes sharper and more distinct.

Determination of Reaction Time

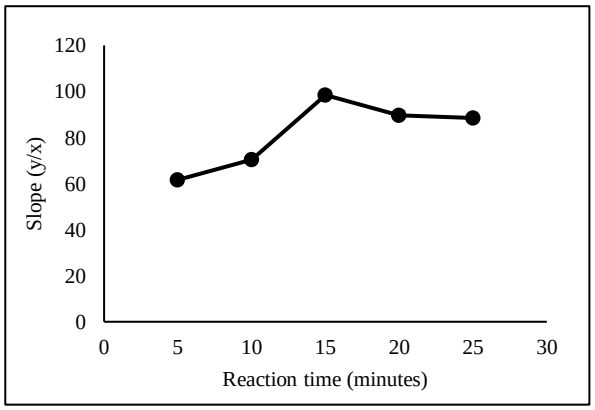

(a)

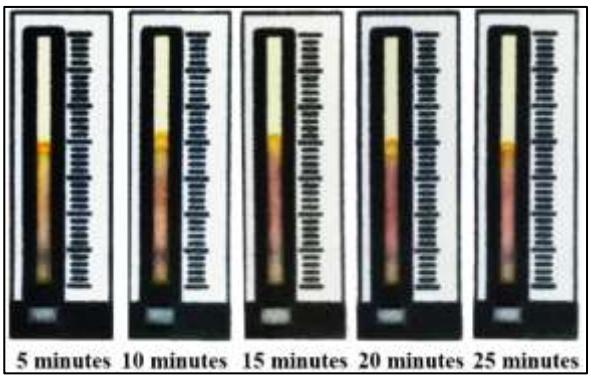

(b)

Figure 9. (a) Graph of the relationship between the average slope value (y/x) and the reaction time, (b) 3D-μPADs image for reaction time.

The determination of reaction time aims to identify the optimal reaction duration for the detection of artificial urine using a mixture of glucose solution and NaOH applied to the sample zone. The results of the reaction time optimization can be seen in **Figure 9**. The optimum reaction time is 15 minutes. At a reaction time of 5 minutes, the resulting color appears faint, indicating that AuNPs are not fully formed. Significant color enhancement is observed at reaction times of 10 and 15 minutes. Prolonged reaction times promote AuNPs formation, consequently influencing the sharpness of the resulting color.

Method Validation

Linearity

Linearity is performed using the previously tested optimization on 3D-μPADs with glucose concentration variations of 0, 20, 40, 60, 80, and 100 mg/dL. Data analysis was carried out using ImageJ software and then processed in Microsoft Excel to measure the length of the reaction distance, resulting in a graph between log concentration (x) and the length of the reaction distance (y). The results of the linearity determination are shown in **Figure 10**.

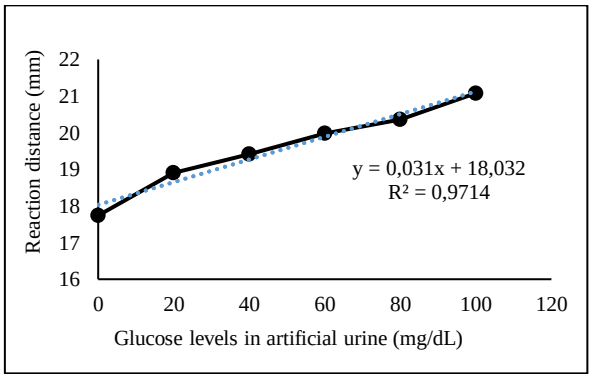

(a)

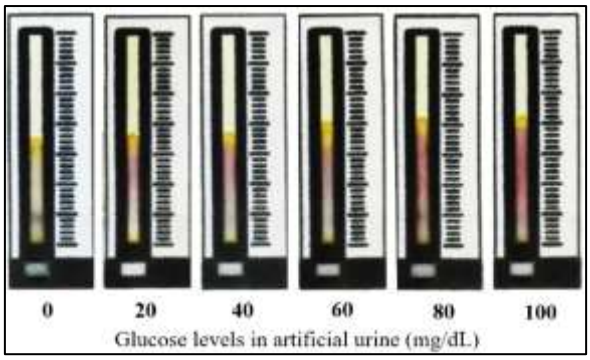

(b)

Figure 10. (a) Graph of the relationship between glucose concentration and length of the reaction distance using imageJ, (b) 3D-μPADs image for linearity.

At a glucose concentration of 0 mg/dL, no color is formed because without glucose, the AuNPs formation reaction cannot occur. The color change becomes visible at glucose concentrations of 20-100 mg/dL, whereas at 20 mg/dL, the color is quite faint. This indicates that the AuNPs formed are also few, but the color sharpness is still clearly visible. The higher the glucose concentration used, the sharper and more distinct

the resulting color. The linear regression correlation obtained with ImageJ software results in a coefficient of determination (R^2) value close to one, which is 0.9714.

Precision

Precision is a method of validation to assess the quality and consistency of measurements performed under identical conditions repeatedly. Precision was performed six times using a glucose concentration of 100 mg/dL in artificial urine. The analysis of the length of the reaction distance was carried out using ImageJ software. The precision test results in a %RSD of 2.69 and a standard deviation (SD) of 0.57.

Accuracy

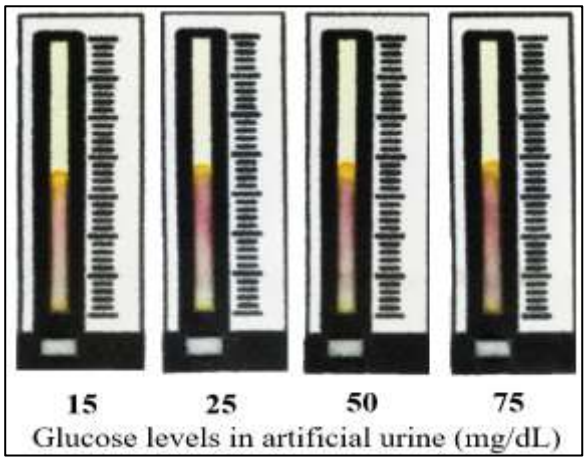

Figure 11. 3D-µPADs image for accuracy.

Accuracy is a method validation to determine the closeness of the measurement to the true value. Accuracy is performed using standard glucose solutions with concentrations of 15, 25, 50, and 75 mg/dL. Data analysis was performed using ImageJ software to obtain the length of the reaction distance. The results are then processed in Ms. Excel to obtain %error and %accuracy. The accuracy test results with ImageJ software produce a higher percentage of accuracy, namely in the range of 92.22-99.23%. The results of the accuracy determination are shown in **Figure 11**.

CONCLUSION

Non-invasive glucose detection can be achieved using 3D-µPADs through AuNPs formation based on color sharpness and reaction distance. AuNPs are one of metal nanoparticles with high biocompatibility and environmental friendliness. The optimization results of 3D-µPADs parameters include a reagent volume of 8 µL, sample volume of 18 µL, drying time of 25 minutes, gold (III) chloride concentration of 75 mM, NaOH concentration of 10 M, and reaction time of 15 minutes. After optimization, method validation for linearity yielded a coefficient of determination (R^2) of 0.9714, precision with %RSD of 2.59, and accuracy in the range of 92.22-99.23%.

ACKNOWLEDGEMENT

We would like to thank the Institute of Research and Community Services Brawijaya University (LPMM) Brawijaya University for the financial support through the 2024 Research Ecosystem Strengthening Grant. Thank to Brawijaya University Facilitating this work.

REFERENCES

[1] Z. Punthakee, R. Goldenberg, and P. Katz, "Definition, classification and diagnosis of diabetes, prediabetes and metabolic syndrome," *Canadian Journal of Diabetes*, **42**, S10–S15, Apr. 2018, https://doi.org/10.1016/j.jcjd.2017.10.003

[2] O. A. Ojo, H. S. Ibrahim, D. E. Rotimi, A. D. Ogunlakin, and A. B. Ojo, "Diabetes mellitus: From molecular mechanism to pathophysiology and pharmacology," *Medicine in Novel Technology and Devices* Sep. 01, 2023, https://doi.org/10.1016/j.medntd.2023.100247

[3] A. T. Kharroubi, "Diabetes mellitus: The epidemic of the century," *World Journal of Diabetes*, **6**(6), 850, 2015, https://doi.org/10.4239/wjd.v6.i6.850

[4] X. Lin *et al.*, "Global, regional, and national burden and trend of diabetes in 195 countries and territories: an analysis from 1990 to 2025," *Scientific Report*, **10**(1), Dec. 2020, https://doi.org/10.1038/s41598-020-71908-9

[5] M. A. B. Khan, M. J. Hashim, J. K. King, R. D. Govender, H. Mustafa, and J. Al Kaabi, "Epidemiology of type 2 diabetes - global burden of disease and forecasted trends," *Journal of Epidemiol Glob Health*, **10**(1), 107–111, Mar. 2020, https://doi.org/10.2991/jegh.k.191028.001

[6] W. V. Gonzales, A. T. Mobashsher, and A. Abbosh, "The progress of glucose monitoring—A review of invasive to minimally and non-invasive techniques, devices and sensors," *Sensors*, **19**(800), 1–45, Feb. 2019, https://doi.org/10.3390/s19040800

[7] K. Khachornsakkul, F. J. Rybicki, and S. Sonkusale, "Nanomaterials integrated with microfluidic paper-based analytical devices for enzyme-free glucose quantification," *Talanta*, **260**(124538), 1–9, Aug. 2023, https://doi.org/10.1016/j.talanta.2023.124538

[8] S. Liu, W. Su, and X. Ding, "A review on microfluidic paper-based analytical devices for glucose detection," *Multidisciplinary Digital Publishing Institute*. Dec. 01, 2016, https://doi.org/10.3390/s16122086

[9] J. Sun, Y. Xianyu, and X. Jiang, "Point-of-care biochemical assays using gold nanoparticle-implemented microfluidics," *Royal Society of Chemistry*, Sep. 07, 2014, https://doi.org/10.1039/C4CS00125G

[10] O. Tokel, F. Inci, and U. Demirci, "Advances in plasmonic technologies for point of care applications," *American Chemical Society*, Jun. 11, 2014, https://doi.org/10.1021/cr4000623

[11] T. Tian, J. Li, Y. Song, L. Zhou, Z. Zhu, and C. J. Yang, "Distance-based microfluidic quantitative detection methods for point-of-care testing," *Royal Society of Chemistry*, Apr. 07, 2016, https://doi.org/10.1039/C5LC01562F

[12] T. Pinheiro *et al.*, "Paper-based in-situ gold nanoparticle synthesis for colorimetric, non-enzymatic glucose level determination," *Nanomaterials*, **10**(10), 1–20, Oct. 2020, https://doi.org/10.3390/nano10102027

[13] T. Pinheiro, A. C. Marques, P. Carvalho, R. Martins, and E. Fortunato, "Paper microfluidics and tailored gold nanoparticles for nonenzymatic, colorimetric multiplex biomarker detection," *ACS Applied Materials and Interfaces*, **13**(3), 3576–3590, Jan. 2021, https://doi.org/10.1021/acsami.0c19089

[14] L. Yang, Z. Zhang, and X. Wang, "A microfluidic PET-based electrochemical glucose sensor," *Micromachines (Basel)*, **13**(552), 1–8, Apr. 2022, https://doi.org/10.3390/mi13040552

[15] Z. Liu, F. Zhao, S. Gao, J. Shao, and H. Chang, "The applications of gold nanoparticle-initialed chemiluminescence in biomedical detection," *Springer New York LLC*, Dec. 01, 2016, https://doi.org/10.1186/s11671-016-1686-0

[16] L. Liang *et al.*, "Aptamer-based fluorescent and visual biosensor for multiplexed monitoring of cancer cells in microfluidic paper-based analytical devices," *Sensors and Actuators B: Chemical*, **229**, 347–354, Jun. 2016, https://doi.org/10.1016/j.snb.2016.01.137

[17] C. Li, Y. Liu, X. Zhou, and Y. Wang, "A paper-based SERS assay for sensitive duplex cytokine detection towards the atherosclerosis-associated disease diagnosis," *Journal of Materials Chemistry B*, **8**(16), 3582–3589, Apr. 2020, https://doi.org/10.1039/C9TB02469G

[18] M. Rahbar, A. R. Wheeler, B. Paull, and M. Macka, "Ion-exchange based immobilization of chromogenic reagents on microfluidic paper analytical devices," *Analytical Chemistry*, **91**(14), 8756–8761, Jul. 2019, https://doi.org/10.1021/acs.analchem.9b01288

[19] Y. Zhang *et al.*, "Distance-based detection of Ag+ with gold nanoparticles-coated microfluidic paper," *Journal of Analysis and Testing*, **5**(1), 11–18, Mar. 2021, https://doi.org/10.1007/s41664-021-00157-0

[20] K. K. Bharadwaj *et al.*, "Green synthesis of gold nanoparticles using plant extracts as beneficial prospect for cancer theranostics," *Molecules*, **26**(6389), 1–41, Nov. 2021, https://doi.org/10.3390/molecules26216389

[21] T. Medina, S. Erlangga, A. Bayu, D. Nandiyanto, and M. Fiandini, "Analisis tekno-ekonomi pada produksi nanopartikel emas (aunp) dengan metode biosintesis menggunakan sargassum horneri pada skala

industri," *Jurnal Teknik Industri (JURTI)*, **1**(2), 103–110, 2022, https://doi.org/10.30659/jurti.1.2.103-110

[22] F. Y. Kong, J. W. Zhang, R. F. Li, Z. X. Wang, W. J. Wang, and W. Wang, "Unique roles of gold nanoparticles in drug delivery, targeting and imaging applications," *Molecules*, **22**(1445), 1–13, Sep. 2017, https://doi.org/10.3390/molecules220914455

[23] E. Ferrari, "Gold nanoparticle-based plasmonic biosensors," *Biosensors (Basel)*, **13**(411), 1–16, Mar. 2023, https://doi.org/10.3390/bios13030411

[24] J. B. Vines, J.-H. Yoon, N.-E. Ryu, D.-J. Lim, and H. Park, "Gold nanoparticles for photothermal cancer therapy," *Front Chem*, **7**(167), 1–16, 2019, https://doi.org/10.3389/fchem.2019.00167

[25] S. Amaliyah, D. P. Pangesti, M. Masruri, A. Sabarudin, and S. B. Sumitro, "Green synthesis and characterization of copper nanoparticles using piper retrofractum vahl extract as bioreductor and capping agent," *Heliyon*, **6**(e0636), 1–12, Aug. 2020, https://doi.org/10.1016/j.heliyon.2020.e04636

[26] G. A. Isola, M. K. Akinloye, Y. K. Sanusi, P. S. Ayanlola, and G. A. Alamu, "Optimizing x-ray imaging using plant mediated gold nanoparticles as contrast agent: A review," *International Journal of Research and Scientific Innovation*, **08**(08), 169–175, 2021, https://doi.org/10.51244/IJRSI.2021.8809

[27] S. Suvarna *et al.*, "Synthesis of a novel glucose capped gold nanoparticle as a better theranostic candidate," *PLoS One*, **12**(6), 1–15, Jun. 2017, https://doi.org/10.1371/journal.pone.0178202

[28] N. J. Lang, B. Liu, and J. Liu, "Characterization of glucose oxidation by gold nanoparticles using nanoceria," *Journal of Colloid and Interface Science*, **428**, 78–83, Aug. 2014, https://doi.org/10.1016/j.jcis.2014.04.025

[29] W. Agudelo, Y. Montoya, and J. Bustamante, "Using a non-reducing sugar in the green synthesis of gold and silver nanoparticles by the chemical reduction method," *DYNA (Colombia)*, **85**(206), 69–78, Jul. 2018, https://doi.org/10.15446/dyna.v85n206.72136